Inverse scheme for acoustic source localization in 3D

Stefan Gombots, Manfred Kaltenbacher
Institute of Mechanics and Mechatronics, TU Wien, Vienna, Austria.

Barbara Kaltenbacher
Institute of Applied Analysis, Alpen-Adria-Universität Klagenfurt, Klagenfurt, Austria.

Summary
Acoustic source localization has become an important task in monitoring and designing products. In the last years, considerable improvements have been achieved in acoustic source localization using microphone arrays. However, main restrictions are given by simplified source models and describing the transfer function between source and microphone signal using Green's function for free radiation. Therefore, reflecting (or partially reflecting) surfaces are not really considered, and the method of using mirror sources is quite limited. To overcome these limitations, we propose an inverse scheme based on a constrained minimization problem. In the provided inverse scheme a cost functional is minimized such that the Helmholtz equation with source terms is fulfilled. This approach aims at finding the position and strength of all sources. The reconstruction is based on solving the corresponding partial differential equation in the frequency domain (Helmholtz equation) by applying the Finite Element Method (FEM) considering the actual boundary conditions as given in the measurement setup. To recover the source location the inverse scheme utilizes a sparsity promoting Tikhonov functional to match measured (microphone signals) and simulated pressure. The applicability and the additional benefit of the inverse scheme compared to frequency domain beamforming will be demonstrated.

PACS no. 43.60.Jn, 43.66.Qp, 43.60.Fg

1. Introduction

Acoustic source localization techniques in combination with microphone array measurements have become an important tool in the development of new products. Moreover, these techniques can be used for failure diagnosis and monitoring as well as for sound design or noise reduction tasks. Thereby, a common technique is acoustic beamforming. It is used to determine source locations and distributions, measure acoustic spectra for complete models and subcomponents, and project results from the array to far field points. Beamforming techniques are based on evaluating simultaneously collected sound pressure data from microphone array measurements. The sound pressure obtained at different microphone positions are mapped to an image of the acoustic source field. This so called beamform map indicates the location and strength of acoustic sources.
The fundamental processing method, Frequency Domain Beamforming (FDBF) [1] is robust and fast. Herein, the beamform map a is computed by

$$a(\boldsymbol{w}) = \bar{\boldsymbol{w}}^T \boldsymbol{C} \bar{\boldsymbol{w}}, \tag{1}$$

with $\boldsymbol{w}$ the steering vector and $\boldsymbol{C}$ the cross spectral matrix of the microphone signals. A bar denotes complex conjugation and ^{T} a transposition. Thereby, a certain model for the acoustic source and sound field is assumed. Most beamforming algorithms models the acoustic source by monopols, so that the transfer function between source and microphone is described by Green's function for free radiation. The steering vectors are therefore given by the free-space Green's function. In literature different formulations of the steering vector can be found [2].
The resolution and the dynamic of FDBF is limited. The theoretical resolution, i. e. the smallest distance of two sources that can be resolved, is usually given through the Rayleigh [3] as well as by the Sparrow limit [4]. The limitation of the resolution and dynamic are caused by the Point Spread Function (PSF) of the microphone array, which is the convolution of the spatial impulse response of the array with a single point source. It has a strong and wide main lobe as well as strong side lobes for low frequencies, so that weaker

sources may be hidden. To overcome these drawbacks, one can use deconvolution techniques, e.g. DAMAS [5], Clean-SC [6] etc., which convert the raw FDBF map (1) into a deconvoluted source map, resulting in higher resolution and dynamic range. In [7] and [8] one can find a detailed comparison between different deconvolution techniques.
However, main restrictions are given by the simplified source model and describing the transfer function between source and microphone using Green's function for free radiation. Therefore, reflecting (or partially reflecting) surfaces are not really considered, and the method of using mirror sources is quite limited. In our approach we solve the corresponding partial differential equation in the frequency domain (Helmholtz equation) with the actual boundary conditions as given in the measurement setup and solve the inverse problem of matching measured (microphone signals) and simulated pressure.
The rest of the paper is organized as follows. In Section 2, the physical and mathematical model will be presented. Afterwards, in Sec. 3 the optimization approach based on the adjoint method and its numerical scheme will be discussed. In Sec. 4 numerical results on a simplified SAE Body in 3D are shown. At the end, the findings are summarized and an outlook to further research will be given.

2. Physical and mathematical model

The physical model is given by the Helmholtz equation in the acoustic domain Ω_{acou}, which is extended by a Perfectly Matched Layer (PML) formulation to mimic the Sommerfeld radiation condition. Therefore, the following generalized form of the Helmholtz equation on $\Omega = \Omega_{\text{acou}} \cup \Omega_{\text{PML}}$ is considered

$$\boldsymbol{\nabla} \cdot \Big(D \boldsymbol{\nabla} p \Big) + b k^2 p = \sigma^{\text{in}} \text{ in } \Omega, \tag{2}$$

where $k \in \mathbb{R}$ denotes the wave number, $\sigma^{\text{in}}(\boldsymbol{x})$ the searched for acoustic sources and

$$D(\boldsymbol{x}) = \begin{cases} \text{diag}\left(\frac{\eta_y(y)\eta_z(z)}{\eta_x(x)}, \frac{\eta_z(z)\eta_x(x)}{\eta_y(y)}, \frac{\eta_x(x)\eta_y(y)}{\eta_z(z)} \right) & \text{in } \Omega_{\text{PML}} \\ 1 & \text{in } \Omega_{\text{acou}} \end{cases}$$

$$b(\boldsymbol{x}) = \begin{cases} \eta_x(x)\eta_y(y)\eta_z(z) & \text{in } \Omega_{\text{PML}} \\ 1 & \text{in } \Omega_{\text{acou}} \end{cases}$$

with appropriately chosen complex valued functions η_x, η_y, η_z (for details see [9]) [1]. On the whole boundary of Ω we impose homogeneous Neumann conditions part of them just as a simple way to close the outer boundary of the PML domain, part of them to model the sound-hard boundary part of the acoustic domain. The weak form of (2) including the Neumann conditions is derived by testing with an arbitrary complex valued function $v \in V$

$$\begin{aligned} &\int_\Omega \Big((D \boldsymbol{\nabla} p) \cdot \boldsymbol{\nabla} \bar{v} - b k^2 p \bar{v} \Big) \, \mathrm{d}\boldsymbol{x} \\ &= - \int_\Omega \sigma^{\text{in}} \bar{v} \, \mathrm{d}\boldsymbol{x} \, \mathrm{d}\boldsymbol{s} \quad \forall v \in V \,, \end{aligned} \tag{3}$$

where a bar over a variable denotes its complex conjugate. In order to include delta pulses as well, we consider not only sound sources as regular functions of the space variable, but as elements of the dual V^*, so that (3) becomes

$$\begin{aligned} A(p,v) \;&=\; \int_\Omega \Big((D \boldsymbol{\nabla} p) \cdot \boldsymbol{\nabla} \bar{v} - b k^2 p \bar{v} \Big) \, \mathrm{d}\boldsymbol{x} \\ &=\; - \langle \sigma^{\text{in}}, \bar{v} \rangle_{V^*,V} \quad \forall v \in V \,. \end{aligned} \tag{4}$$

Now, the considered inverse problem is to reconstruct σ^{in} from pressure measurements

$$p_i^{\text{ms}} = p(\boldsymbol{x}_i) \,, \quad i = 1, \ldots, M \tag{5}$$

at the microphone positions $\boldsymbol{x}_1, \ldots, \boldsymbol{x}_M$. For the acoustic sources we make the following ansatz

$$\sigma^{\text{in}} = \sum_{j=1}^{N} a_j e^{i\varphi_j} \delta_{\boldsymbol{x}_j} \tag{6}$$

with the searched for amplitudes $a_1, a_2, ..., a_N \in \mathbb{R}$ and phases $\varphi_1, \varphi_2, ..., \varphi_N \in [-\pi/2, \pi/2]$. Here, N denotes the number of possible sources and $\delta_{\boldsymbol{x}_j}$ the delta function at position $\boldsymbol{x}_j$.

3. Optimization based source identification

The following constrained optimization problem by means of Tikhonov regularization have to be solved

$$\begin{aligned} &\min_{p \in U, a \in \mathbb{R}^N, \varphi \in [-\frac{\pi}{2}, \frac{\pi}{2}]^N} J(p,a,\varphi) \;\; \text{s.t. } \forall v \in V : \\ &A(p,v) = -\text{Re}\left(\sum_{j=1}^{N} a_j e^{i\varphi_j} \delta_{\boldsymbol{x}_j} \right) \end{aligned} \tag{7}$$

where $a = (a_1, \ldots, a_N)$, $\varphi = (\varphi_1, \ldots, \varphi_N)$ and

$$\begin{aligned} J(p,a,\varphi) \;=\; &\frac{1}{2} \sum_{i=1}^{M} |p(\boldsymbol{x}_i) - p_i^{\text{ms}}|^2 \\ &+ \alpha \sum_{j=1}^{N} \Big| a_j \Big|^q + \beta \sum_{j=1}^{N} \varphi_j^2 \,. \end{aligned}$$

To pick the few true source locations from a large number N of trial sources sparsity of the reconstruction is desired. One can enhance sparsity, when the

[1] Since the identification is done separately for each fixed frequency, the dependency on ω is neglected in the notation.

exponent $q \in (1,2]$ is chosen close to one [10]. Furthermore, the regularization parameters α, β are chosen according to the sequential discrepancy principle [11], where $\beta = \alpha = \alpha_0 2^{-m}$ with m the smallest exponent such that following inequality

$$\sqrt{\sum_{i=1}^{M} (p(\boldsymbol{x}_i) - p_i^{\mathrm{ms}})^2} \leq \varepsilon \tag{8}$$

is fulfilled. Here, ε denotes the measurement error. We can expect this to lead to a convergent regularization method [12].

In a next step, we want to derive the first order optimality conditions and consider the following Lagrange functional

$$\begin{aligned}\mathcal{L}(a,\varphi,p,z) \;=\; & J(p,a,\varphi) + A(p,z) \\ & + \sum_{j=1}^{N} a_j \mathrm{Re}\left(e^{i\varphi_j}\delta_{\boldsymbol{x}_j}\right) ,\end{aligned}$$

with some adjoint state z. Due to regularity of the constraint a minimizer has to satisfy the following optimality conditions:

$$0 = \frac{\partial \mathcal{L}}{\partial a_j}(a,\varphi,p,z) \tag{9}$$

$$0 = \frac{\partial \mathcal{L}}{\partial \varphi_j}(a,\varphi,p,z) \tag{10}$$

$$0 = \frac{\partial \mathcal{L}}{\partial p}(a,\varphi,p,z)[w] \tag{11}$$

$$0 = \frac{\partial \mathcal{L}}{\partial z}(a,\varphi,p,z)[v]. \tag{12}$$

The fourth optimality condition (12) is just the state equation (7), whereas (11) is the adjoint equation for $z = z(a,\varphi)$, whose strong form (in terms of $\bar{z}$) is

$$\begin{aligned}\boldsymbol{\nabla}\cdot D\boldsymbol{\nabla}\bar{z} + bk^2\bar{z} \;&=\; -\sum_{i=1}^{M}(p(\boldsymbol{x}_i) - p_i^{\mathrm{ms}})\delta_{\boldsymbol{x}_i} \quad \text{in } \Omega \\ \boldsymbol{n}\cdot D\boldsymbol{\nabla}\bar{z} \;&=\; 0 \quad \text{on } \partial\Omega\,. \end{aligned} \tag{13}$$

To carry out, e.g., some gradient method for solving this optimality system, the gradient of the reduced cost functional is computed via

$$\begin{aligned}\frac{\partial j}{\partial a_i}(a,\varphi) &= \frac{\mathrm{d}}{\mathrm{d}a_i}\Big(J(p(a,\varphi),a,\varphi)\Big) \\ &= \frac{\mathrm{d}}{\mathrm{d}a_i}\Big(\mathcal{L}(p(a,\varphi),a,\varphi,z(a,\varphi))\Big) \\ &= \frac{\partial \mathcal{L}}{\partial p}(p(a,\varphi),a,\varphi,z(a,\varphi))\frac{\partial p}{\partial a_i}(a,\varphi) \\ &\quad + \frac{\partial \mathcal{L}}{\partial a_i}(p(a,\varphi),a,\varphi,z(a,\varphi)) \\ &\quad + \frac{\partial \mathcal{L}}{\partial z}(p(a,\varphi),a,\varphi,z(a,\varphi))\frac{\partial z}{\partial a_i}(a,\varphi) \\ &= \frac{\partial \mathcal{L}}{\partial a_i}(p(a,\varphi),a,\varphi,z(a,\varphi))\,.\end{aligned}$$

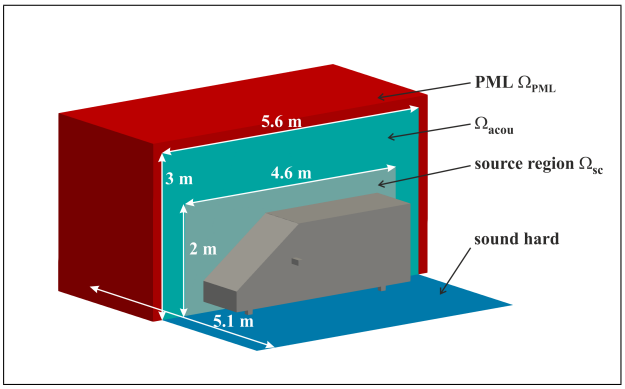

Figure 1. Computational setup.

Analogously, the derivative w.r.t φ_i have to be performed. Due to the special choice of amplitude and phase in (6), we obtain for the actual physical quantities

$$\text{Amplitude}: |a_j|$$

$$\text{Phase}: \begin{cases} \varphi_j & \text{if } \varphi \geq 0 \\ \varphi_j + 2\pi & \text{if } \varphi < 0 \end{cases} \quad \text{if } a_j > 0$$

$$\varphi_j + \pi \qquad\qquad \text{if } a_j < 0\,.$$

For the practical realization, a minimization by a gradient method with Armijo line search is applied.

4. Numerical results

To demonstrate the applicability of the inverse scheme in 3D, we chose a numerical example that is similar to a setup in wind tunnel measurements, see Fig. 1. It consists of a simplified SAE Type 4 body [13], where two acoustic sources with equal intensity are positioned. One source is placed near the side mirror and one near the wheel housing. The frequency of both sources was chosen to 500 Hz. The floor is fully reflective (sound hard) as well as the SAE body. To approximate free radiation, a perfectly matched layer (PML) on the remaining five sides is used. The speed of sound is assumed to be 343 m/s. To get realistic pressure values at the microphone positions, we perform a forward simulation on a much finer computational grid as then used for the identification process. The fine grid had approximately 4.6 million degrees of freedom, whereas the coarse grid used for the inverse scheme had about 0.5 million degrees of freedom. We also made the PML region of the fine grid twice as thick than on the coarse grid. Additionally, random noise was added to the simulated pressure data resulting in a signal to noise ratio of 26 dB. Moreover, the microphone positions in the fine and coarse differ slightly from each other to get a realistic situation. Thereby three different microphone configurations have been considered for the source localization.

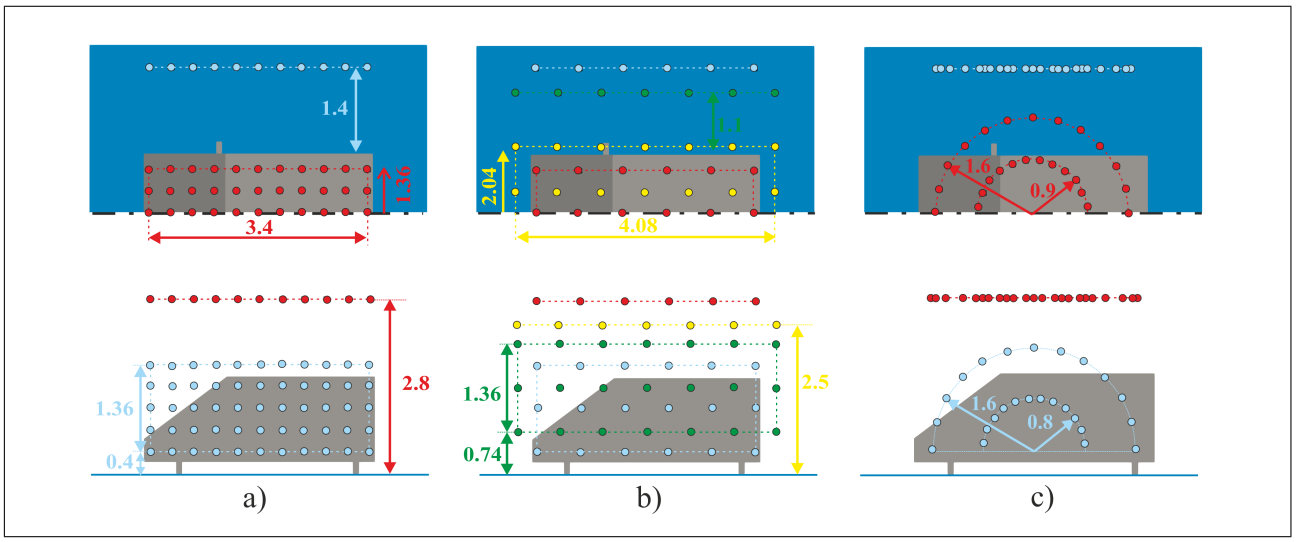

Figure 2. Different microphone configurations (dimension in m).

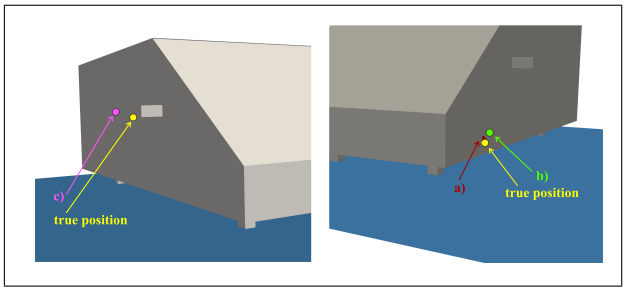

Figure 3. Localization results using Clean SC.

Table I. Localization results (detail).

Source	Wheel			Mirror		
Config.	x	y	z	x	y	z
original	1.30	0.30	-1.00	0.70	0.90	1.25
a)	1.30	0.33	-0.97	-	-	-
b)	1.30	0.39	-1.04	-	-	-
c)	-	-	-	0.70	0.95	1.40

The configurations are depicted in Fig. 2. In configuration a) three grid arrays with in total 165 microphones were used. These equally spaced microphone arrays (spacing of 0.34 m) were placed left, right and over the simplified SAE Body. Additionally, in configuration b) another three grid arrays were placed left, right and over the body, but at different planes (in total there are 124 microphones). Also the grid spacing for the arrays were increased from 0.34 m to 0.68 m. At the third configuration c) 98 microphones on two circle and four semicircle arrays were used.

First of all, a beamforming algorithm was used to identify the acoustic sources in the source region. Hereby, meaningful results in 3D can be achieved by deconvolution algorithms like Clean-SC [6]. In Fig. 3 one can see the results using the three different microphone arrangements. Due to the fact that the two acoustic sources are coherent, the algorithm just will find one of the sources. Looking at Tab. I the localization results in detail are given and one can see that Clean SC performs quite well. However, the real source distribution (see Fig. 4 (*top-left*)) can not be reconstructed and also the phase information is lost. Further, using identified sources from beamforming algorithms to reconstruct the sound pressure field will led to wrong results.

Next, the applicability of the inverse scheme in 3D is demonstrated. To this end, the regularization parameters were set to $\alpha = 0.125$ and $\beta = 0.125$. For the exponent q, the value 1.1 was chosen to favor sparse reconstruction. The searched for sources are modeled by delta peaks for each of the 105.651 nodes within the source region Ω_{sc}. The implemented optimization based parameter identification algorithm is based on a gradient method with Armijo line search exploring the adjoint method to efficiently obtain the gradient of the objective function. The maximum number of reducing the regularization parameters were set to 15. To identify the acoustic source from the simulated pressure values the total elapsed CPU time (stand-alone PC with an Intel Xeon E5-2697A, 2.60 GHz processor) was about 74 hours. The results of the reconstruction with the different microphone configurations are depicted in Fig. 4. As one can see, the source distribution was reconstructed in a good manner. Here, the best result was achieved by configuration b) with the microphones at different planes. One can see that there are the fewest source artefacts. Hence, the microphone positions and the number of microphones are important for the quality of the identification. Next, using the identified source distribution and performing a sound field computation gives the acoustic fields displayed in Fig. 5. Here, configuration a) and b) provide a good

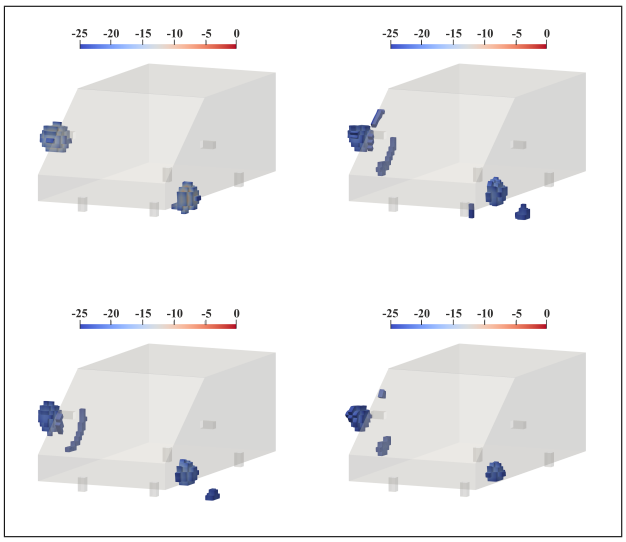

Figure 4. Amplitude of the source normalized the to source strength of the original source (unit in dB) (*top-left*) Original source (*top-right*) Identified source with a) (*bottom-left*) Identified source with b) (*bottom-right*) Identified source with c).

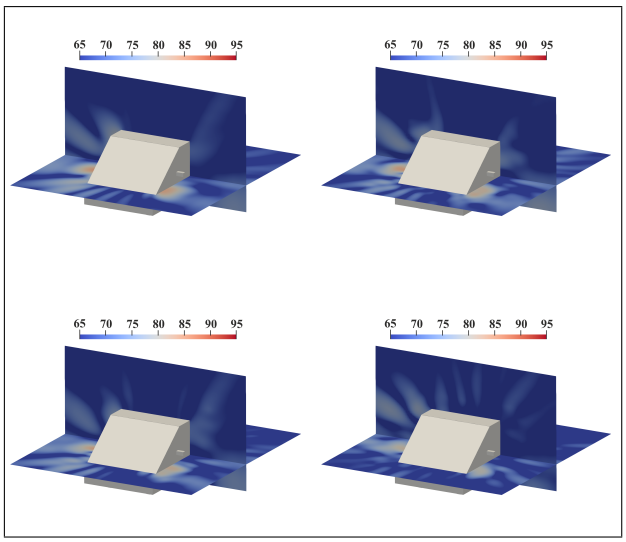

Figure 5. Computed acoustic sound pressure level (*top-left*) Original sources (*top-right*) Identified sources with a) (*bottom-left*) Identified sources with b) (*bottom-right)* Identified sources with c).

Table II. Relative L^2 error between measured and computed pressure values at the microphone positions.

Configuration	a)	b)	c)
Error	2.93%	2.05%	5.54%

agreement with the original sound field. To quantify the achieved error the deviation between the acoustic pressure at the microphone positions was computed according to (8) and normalized to the L^2-norm of the measured pressure values (see Tab. II).

These results demonstrate the applicability of the inverse scheme in 3D. Hereby, the best agreement between the original and computed sound field was achieved by configuration b). A spatial distribution of the microphones around the sound source could also improve the localization result, therefore the question of optimal positioning of the microphones arises.

5. Conclusion and Outlook

Results of the inverse scheme in 3D were presented, which offers promising source identification. Our first numerical results in 3D demonstrates the potential of the approach and the applicability to the low frequency range, where the classical beamforming algorithms are limited. A big advantage in a simulation based identification is, that it allows to appropriately treat boundary conditions in realistic experimental setups. In a next step, we will perform measurements for real world situation and will apply the developed inverse scheme. Hereby, the determination of the boundary conditions may be the most challenging fact. Further, investigations in the optimal positioning of the microphones will also be done to improve the results of the source identification.

References

[1] T. J. Mueller: Aeoroacoustic measurements. Springer-Verlag Berlin Heidelberg, 2002.

[2] E. Sarradj: Three-dimensional acoustic source mapping with different beamforming steering vector formulations. Advances in Acoustics and Vibration, Volume 2012, Article ID 292695.

[3] D. H. Johnson, D. E. Dudgeon: Array signal processing: concepts and techniques. PTR Prentice Hall Englewood Cliffs, 1993.

[4] R. P. Dougherty, R. C. Ramachandran, G. Raman: Deconvolution of sources in aeoroacosutic images from phased microphone arrays using linear programming. International Journal of Aeoroacoustics, 12 (2018), 699-717.

[5] T. F. Brooks, W. M. Humphreys: A deconvolution approach for the mapping of acoustic sources (damas) determined from phased microphone arrays. Journal of Sound and Vibration, 294 (2006), 856-879.

[6] P. Sijtsma: CLEAN based on spatial source coherence. International Journal of Aeroacoustics, Vol. 6, 4 (2007), 357-374.

[7] Z. Chu, Y. Yang: Comparison of deconvolution methods for the visualization of acoustic sources based on cross-spectral imaging function beamforming. Mechanical System and Signal Pocessing, 48 (2014), 404-422.

[8] T. Padois, A. Berry: Two and Three-Dimensional Sound Source Localization with Beamforming and Several Deconvolution Techniques. Acta Acustica united with Acoustica, 103 (2017), 357-392.

[9] M. Kaltenbacher: Numerical Simulation of Mechatronic Sensors and Actuators: Finite Elements for Computational Multiphysics, 3 ed. Springer-Verlag Berlin Heidelberg, 2015.

[10] A. Schuhmacher, K. Rasmussen, C. Hansen: Sound source reconstruction using inverse boundary element calculations. Journal of the Acoustical Society of America, 113 (2003), 114-127.

[11] S. W. Anzengruber, B. Hofmann, P. Mathé: Regularization properties of the sequential discrepancy principle for Tikhonov regularization in Banach spaces. Applicable Analysis, 93 (2014), 1382-1400.

[12] S. Lu, S. V. Pereverzev: Multi-parameter regularization and its numerical realization. Numerische Mathematik, 118 (2011), 1-31.

[13] Society of Automotive Engineers: Aerodynamic Testing of Road Vehicles in Open Jet Wind Tunnels. SAE Special Publication 1465 (1999).